Scaling and Distilling Transformer Models for sEMG

Anonymous authors
Paper under double-blind review

Abstract

Surface electromyography (sEMG) signals offer a promising avenue for developing innovative human-computer interfaces by providing insights into muscular activity. However, limited available training data and computational constraints during deployment have restricted the use of state-of-the-art machine learning models, such as transformers, in challenging sEMG tasks. In this paper, we demonstrate that transformer models can learn effective and generalizable representations from sEMG datasets that are small by modern deep learning standards (approximately 100 users), surpassing the performance of classical machine learning methods and older neural network architectures. Additionally, by leveraging model distillation techniques, we reduce parameter counts by up to 50x with minimal loss of performance. This results in efficient and expressive models suitable for complex real-time sEMG tasks in dynamic real-world environments.

1 Introduction

Recently, there has been growing interest in using surface electromyography (sEMG) in conjunction with powerful deep learning techniques to decode human muscle activity (e.g. Di Nardo et al., 2022; Gaso et al., 2021; Wimalasena et al., 2022; Buongiorno et al., 2021; Ozdemir et al., 2020). sEMG offers the potential for novel human-computer interfaces (HCIs), where user gestures or movements can serve as direct control input (CTRL-labs at Reality Labs, 2024). Advances in hardware (e.g. Lu et al., 2024; CTRL-labs at Reality Labs, 2024) have now made it feasible to reliably capture sEMG outside of a controlled clinical setting. Supported by these developments, deep learning methods have been applied to a variety of EMG tasks, including muscle activation detection (Di Nardo et al., 2022), (Wimalasena et al., 2022), gesture classification (Atzori et al., 2016), (He et al., 2018), (Zhang et al., 2023), and speech recognition (Wand & Schmidhuber, 2016).

However, there are a few limitations in previous works. First, these approaches frequently do not employ cutting-edge model architectures, such as transformers, or apply them only to limited time scales, such as single isolated gestures (e.g., Ozdemir et al., 2020; He et al., 2018). This limitation may be due to the restricted quantity and/or diversity of available training data (Li et al., 2021), as large-scale data is often viewed as a prerequisite for applying contemporary deep-learning methods to complex tasks. Nonetheless, meeting the needs of a functional HCI requires modeling non-stationary and noisy sEMG data (Cochrane-Snyman et al., 2016; Chowdhury et al., 2013), a challenge likely better suited to more sophisticated models. A second consideration commonly unaddressed in previous works is the computational challenges associated with running an HCI in the wild. In particular, there are likely to be substantial constraints on the model size (small enough to run on an edge device) and inference time (fast enough for the system to be responsive). Finally, the ability to effectively generalize to unseen users is critical to successful deployment in real-world applications, yet evaluation on unseen users is often neglected in the existing literature.

In this paper, we take steps towards addressing these challenges:

1. We demonstrate that transformer models can, in fact, learn effectively on small (by deep learning standards) sEMG datasets, with approximately 350 hours of data collected from around 100 users, even on a challenging task like *emg2qwerty* (Sivakumar et al., 2024). A small transformer (2.2M parameters) outperforms the SOTA performance on this task by about 20% (absolute). We further show that the performance of the transformer models improves with model scale, enabling us to

improve the SOTA performance by over 25% (absolute). Although the community has largely used simpler modeling techniques like Random Forests (Rani et al., 2024) or RNNs (He et al., 2018) on handcrafted features, and has avoided data-hungry transformers, our findings suggest that transformers applied directly to sEMG signal can work well even at this data scale.

2. We demonstrate that model distillation (Hinton et al., 2015), which transfers knowledge from a large pre-trained 'teacher' model to a smaller 'student' model, can be effectively applied to sEMG data. We show that training larger transformer models followed by distillation into smaller models substantially outperforms direct training of the small-sized transformer without distillation, reducing the parameter count of the transformer model by up to 50x with minimal performance degradation ($< 1.5\%$ absolute). To date, there has been limited work towards distilling sEMG models.

3. Unlike most previous works, which focused on reporting performance on a set of held-out *trials* from the 'seen' (during training) users, we focus on the much more realistic and challenging setup - reporting performance on the 'heldout' (during training) users.

We release the code used for training and distilling the models to make it easier for the scientific community to reproduce our results and build on top of this work.

2 Background

2.1 Surface Electromyography

The human central nervous system initiates muscular activity by transmitting an electrical impulse along a nerve bundle (Plonsey & Barr, 2007; CTRL-labs at Reality Labs, 2024). Surface electromyography (sEMG) uses external electrodes to measure these electrical action potentials as they propagate from the nerve fiber to the motor unit (Mokhlesabadifarahani & Gunjan, 2015; CTRL-labs at Reality Labs, 2024). sEMG data is noisy and non-stationary (Chowdhury et al., 2013; Cochrane-Snyman et al., 2016), making it a difficult signal modality for machine learning tasks. Better modeling sEMG has potential applicability to other electrophysiological data modalities, including EEG and EKG (Brambilla et al., 2021; Li et al., 2023; Yang et al., 2023)

Due to the difficulty of collecting EMG data, most open-source EMG datasets are small in terms of users and total recording time. Furthermore, most focus on capturing isolated movements that are relatively distinct from one another, such as the flexion of different fingers. For example, despite being some of the largest and most popular sEMG datasets, the Ninapro (Atzori et al., 2014) corpus is predominantly focused on recognizing isolated gestures and contains only 77 subjects in its largest dataset. The EPN dataset (Benalcazar et al., 2020) is much larger but still focuses on simple enough gesture recognition such that relatively simple models seem to saturate performance on it. Most other datasets, such as Amma et al. (2015) (5 subjects) and Ortiz-Catalan et al. (2013) (17 subjects), are even smaller and still primarily based on single-gesture/movement recognition. In contrast, an effective human-computer interface (HCI) should have the ability to disentangle multiple sequential gestures (that may overlap each other) and generalize across a diverse set of users.

Improving on the above, recently Sivakumar et al. (2024) released a dataset that represents a significant advancement over existing sEMG benchmarks in terms of its scale, task complexity, and real-world applicability. As described in Figure 1, the task is to predict key presses while touch typing on a keyboard using sEMG activity alone. The dataset captures dynamic typing behavior across 108 users and $1,135$ sessions totaling 346 hours of high-resolution wrist-based sEMG recordings. The naturalistic, high-dimensional output space (key pressed on a keyboard) and the larger data scale make it suitable for studying both cross-user zero-shot generalization and personalized finetuning on unseen (during training) users. For these reasons, we focus on this dataset in our experiments.

As a result of both limited data availability and the inherent challenges of the modality (e.g., noise, subject-based variance), prior works have tended to utilize classical approaches for sEMG tasks. In some, simple machine learning approaches such as support vector machines, random forests, K-nearest-neighbors or linear

Reference	Task	Number of participants	Model
(She et al., 2010)	Lower-limb movt.	3	SVM
(Alkan & Günay, 2012)	Upper-arm movt	Not Reported	SVM
(Atzori et al., 2016)	Hand gesture	78	CNN
(Wand & Schmidhuber, 2016)	Speech recog.	4 dev, 7 eval	DNN + HMM
(He et al., 2018)	Hand gesture	27	LSTM + MLP
(Cai et al., 2018)	Facial expr.	7	SVM
(Xia et al., 2018)	3D limb motion est.	8	CNN + RNN
(Shioji et al., 2018)	Auth., hand gesture	8	CNN
(Morikawa et al., 2018)	Authentication	6	CNN
(Ozdemir et al., 2020)	Hand gesture	30	CNN (ResNet-50)
(Rahimian et al., 2021)	Hand gesture	40	Transformer
(Gaso et al., 2021)	Myopathy, ALS det.	25	FC-DNN
(Godoy et al., 2022)	Hand gesture	10	VIT
(Di Nardo et al., 2022)	Muscle activation	18 + 30	FC-DNN
(Chen et al., 2023)	Finger joint est.	12	Transformer
(Zabihi et al., 2023)	Hand gesture	40	Transformer
(Zhang et al., 2023)	Hand gesture	20	LSTM + Transf.
(Liu et al., 2024)	Hand gesture	50	CNN + VIT
(Rani et al., 2024)	Hand gesture	8 + Not Reported + 6	RF, KNN, LDA
(Putro et al., 2024)	Finger joint est.	5	Transformer
(Eddy et al., 2024)	Hand gesture	612	RNN
(Sivakumar et al., 2024)	Typing	108	TDS-ConvNet

Table 1: Prior work: most datasets are relatively small, and often classical ML approaches or older neural network architectures are used. When number of participants is of the format X + Y, different devices or protocols were used so that they cannot be trivially combined into one dataset. In some cases, the number of participants is not reported in the papers and we denote them as 'Not Reported'. Most of these prior works have not evaluated their models on unseen users.

discriminant analysis are used (Rani et al., 2024; Atzori et al., 2014). In others, models such as CNNs (Ozdemir et al., 2020; Atzori et al., 2016) and LSTMs (He et al., 2018) have been applied, primarily for gesture classification on a restricted set of users. Some recent work has begun to explore the application of transformer-based models (Chen et al., 2023; Putro et al., 2024; Zabihi et al., 2023; Zhang et al., 2023) and vision transformers (ViTs) to sEMG data (Rahimian et al., 2021; Godoy et al., 2022; Liu et al., 2024), but these efforts are also limited to small-scale datasets and simpler tasks. In addition, prior methodologies primarily use manual feature extraction techniques on sliding windows of the sEMG signals, e.g., spectrograms (Sivakumar et al., 2024), multivariate power frequency features(CTRL-labs at Reality Labs, 2024), Hjorth parameters (Rani et al., 2024) and others. We instead focus on learning transformer-based models that uses learned sEMG featurization directly from the raw data, as is popular in other modalities.

Finally, the existing literature often falls short in addressing a critical aspect of training data on sEMG data: cross-user generalization. It is well-established that sEMG signals, like other bio-signals, exhibit high inter-individual variability (Chowdhury et al., 2013; CTRL-labs at Reality Labs, 2024), making it essential to evaluate the robustness of models on "unseen" (heldout during training) users. However, many prior works neglect this crucial consideration, instead opting to test their models solely on held-out *trials* from the same individuals contained within the training set, thus failing to provide a meaningful assessment of

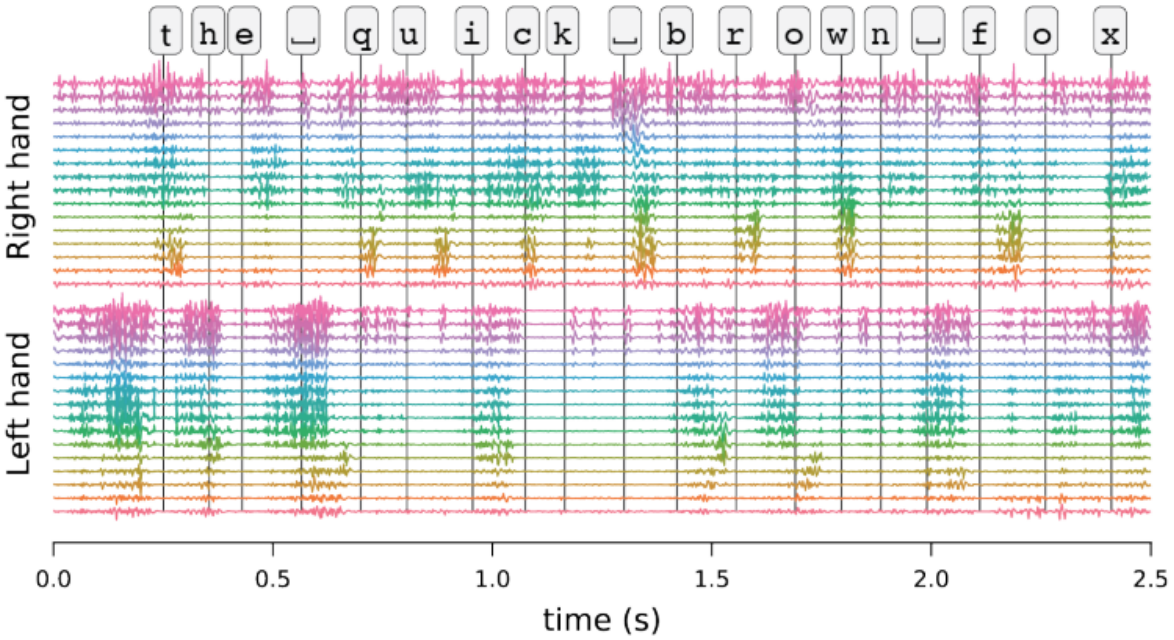

Figure 1: The *emg2qwerty* task: participants type on a keyboard while sEMG activity is recorded from both hands. The goal is to map from sequences of sEMG signals to sequences of characters. Figure cropped from `https://github.com/facebookresearch/emg2qwerty`, licensed CC BY-NC-SA.

the model's ability to generalize across diverse users. We focus our evaluation on new participants unseen in the training set.

Table 1 reviews recent work in the domain of sEMG decoding, showing that for the most part, datasets used are small (<100 participants, or even <10) and modeling techniques used are often classical and data-efficient.

2.2 Distillation

Model distillation was popularized by (Hinton et al., 2015), who proposed training a small 'student' model on the outputs (logits) of a larger pretrained 'teacher' model, along with the ground-truth labels from the training data. This improved the performance of the smaller 'student' model compared to the case where the smaller model was trained from scratch. Subsequent works have hypothesized that distillation helps because the 'teacher' model's logits provide information about interclass relationships (Tang et al., 2020) as well as sample difficulty (Zhao et al., 2022).

Some works go beyond using outputs or logits alone for distillation, especially for deeper models. These approaches drive the 'student' model intermediate layer representations 'close' to the intermediate layer representations in the 'teacher' model (Romero et al., 2015). In practice, this is achieved by regularizing the 'distance' (e.g. ℓ_1, ℓ_2) between the activations of the 'teacher' and the 'student' model for pre-determined pairs of layers. In case of a mismatch between the shape of the layers, linear regression can be used to align the dimensions. These 'feature-based' distillation methods have been successfully used to distill large foundation models like HuBERT with minimal performance degradation (Lee et al., 2022; Peng et al., 2023; Wang et al., 2023). Komodakis & Zagoruyko (2017) proposed applying a function that maps hidden representation of a CNN to a 2-D attention map and training the 'student' model to imitate the attention map from the 'teacher' instead of the features from the 'teacher'. Chen et al. (2021) eliminates the need for ad-hoc mapping functions by learning the optimal 'student-to-teacher' mapping layer. In contrast to directly minimizing some form of distance measure, Xu et al. (2018) proposed training an adversarial discriminator network to distinguish between the representations from the 'teacher' and the 'student'.

Even more sophisticated approaches encode 'teacher' knowledge in higher-order relationships between multiple samples. For example, Tung & Mori (2019) proposed computing an inner-product-based similarity matrix between a batch of samples for both the 'teacher' and 'student' models and then training the student to match the teacher's matrix. A similar approach was presented by Park et al. (2019), which explored both Euclidean and angular similarity metrics. However, the benefits of these relational distillation methods are marginal compared to feature-based approaches, especially considering the added computational complexity.

In this work, our focus is on showing that distillation methods can be applied out-of-the-box on sEMG. Given that logit distillation is a simple and widely used technique, we use this technique in our experiments.

3 Experiments

We design experiments to demonstrate that: **i)** Transformer models can be effective for sEMG tasks even when considering datasets and models that are small by modern deep learning standards; **ii)** The performance of the transformer models further improves with scale, resulting in improvements to SOTA performance; **iii)** Transformer models can be distilled into smaller-sized models, recovering most of the large-model performance with 50x fewer parameters. We primarily focus on zero-shot performance on held-out users, and additionally report personalization performance (where a model is fine-tuned on a small amount of a held-out single-user's data, then evaluated on held-out sessions from that user). Both cross-user generation and personalization are key challenges for real-world sEMG tasks (CTRL-labs at Reality Labs, 2024).

3.1 Dataset

We use the *emg2qwerty* dataset (Sivakumar et al., 2024) in our experiments. The dataset consists of two-handed sEMG recordings from users typing on a computer keyboard. The data is labeled with the corresponding keystrokes, and the task is to map from sEMG sequences to character sequences. Figure 1 shows a representative example. In total, the dataset contains 346 hours of sEMG recordings across 108 unique users. The dataset is split into 100 users for training and validation and 8 held-out users for testing. For each user, we hold out 2 validation sessions and 2 testing sessions, then use the rest for training. In the generic setting, we train on the 100 user training set, validate on the 100 user validation set and evaluate on the 8 user testing set. In the personalization setting, for each of the 8 users, we train on their individual training set, then validate and test on their respective validation and testing set. Sessions are windowed to form 4 second samples, padded with an additional 900 ms of past context and 100 ms of future context.

3.2 Models

Our baseline is the Time-Depth Separable Convolutional Network (TDS-ConvNet) model introduced in Hannun et al. (2019) and used by Sivakumar et al. (2024), which reports that the parameter-efficiency of TDS-ConvNet allows for wider receptive fields which have proven important in *emg2qwerty* modeling. We use the same train, validation, and test splits as used in Sivakumar et al. (2024) and report the performance of the baseline models from that paper.

Our model architecture consists of a convolutional featurizer followed by a transformer encoder and a linear decoder. The featurizer always uses 3 convolutional layers, with instance norm applied along the time axis after the first convolutional layer, and downsamples the input sEMG data (which is sampled at 2kHz) to a sequence of features (sampled at 100 Hz). The encoder consists of a series of Transformer blocks (Vaswani et al., 2017) whose number and width we manipulate to create larger or smaller models. The transformer blocks use causal attention so that they can be used in an online streaming setup. The linear decoder converts the transformer's output to a sequence of logits. Note that unlike Sivakumar et al. (2024) which uses log-spectrograms as input features, we train our model end-to-end using raw sEMG data directly, without using any hand-designed feature engineering pipeline. Following Sivakumar et al. (2024), during training we apply channel rotation, which randomly shifts the sEMG channels by ± 1 as a data augmentation technique to simulate different spatial orientations of the device.

We have trained 20 different architectures, generated by permuting [2, 4, 6, 8, 10] layers and inner dimension of [128, 256, 512, 1024]. The ratio of the transformer inner dimension and the transformer feed-forward dimension is fixed at four. While we report on performance of all models in the supplement, for ease of exposition in the main text, we are concerned with three 'reference' architectures: the TINY architecture consisting of 10 layers of inner dimension 128 (about 2.2M parameters); the SMALL architecture consisting of 6 layers of inner dimension 256 (about 5.4M parameters, close to the 5.3M TDS-ConvNet baseline); and the LARGE architecture consisting of 8 layers of inner dimension 1024 and about 109M parameters. We use the AdamW optimizer(Loshchilov, 2017) for training all models. In the figures we additionally include other models along the size-performance Pareto frontier (i.e. ones which perform better than any model of the same or lesser parameter count). For all the experiments, we report standard deviation across multiple seeds (6 seeds for supervised training of transformer models, 3 seeds for personalization experiments, and 3 seeds for distillation experiments).

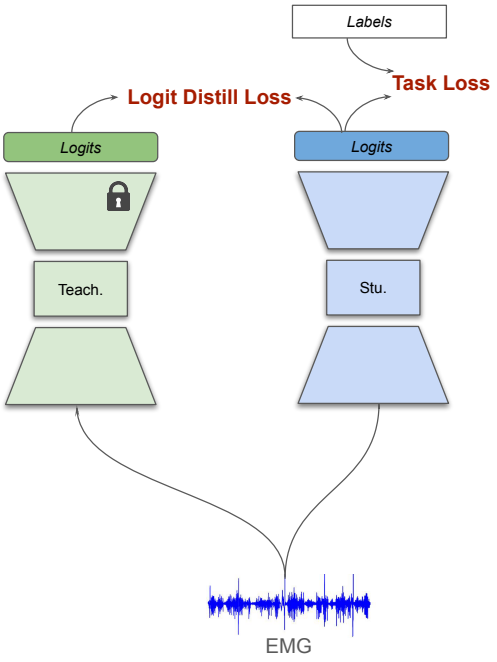

Figure 2: An illustration of the distillation process: the smaller student model receives training signal from the logits of the larger teacher model in addition to the regular supervised loss.

3.2.1 Supervised training of transformer models

Following Sivakumar et al. (2024), we use the connectionist temporal classification (CTC) loss (Graves et al., 2006) to train the transformer models on the *emg2qwerty* task. We train the transformer models on a single V100 node (8 32Gb GPUs) using cosine learning-rate scheduling (Loshchilov & Hutter, 2017) and linear learning rate warmup for first 5% of updates. We document all the hyperparameters in the Appendix in Section A.

3.2.2 Model distillation

We use logit distillation to distill the pretrained LARGE teacher model into a set of smaller (but differently sized) student models. For the student models, we include all 20 architectures discussed above (including ones of the same size as the teacher). This enables us to demonstrate the benefits of distillation at varying student model sizes. The process is depicted in Figure 2.

The distillation loss $\mathcal{L}_{\text{distill}}$ is the cross-entropy loss where the student's output probabilities at each time step are expected to match the soft targets provided by the teacher's per-timestep output probabilities. We use a temperature scaling factor of 2 when computing the probabilities. The distillation loss is then combined with the task loss (i.e. CTC) to give the final training loss for the student model:

$$\mathcal{L} = \frac{1}{\alpha + \beta}\left(\alpha \mathcal{L}_{\text{distill}} + \beta \mathcal{L}_{\text{task}}\right).$$

Here, α and β are hyperparameters. We set $\beta = 1.0$ and experimented with α values between 0.1 and 1.0. The optimal value of different hyperparameters is documented in the Appendix.

3.3 Metrics

Following (Sivakumar et al., 2024), we evaluate the *emg2qwerty* models using Character Error Rate (CER), defined as the Levenshtein edit-distance between the predicted and the ground-truth sequence. It can be expressed as $\frac{(S+D+I)*100}{N}$ where, given the predicted and the ground-truth sequences, S is the number of

Benchmark	Architecture	Parameters	CER (↓%)
Generic	TDS-ConvNet	5.3M	55.57
	Tiny Transformer	2.2M	35.9± 0.9
	Small Transformer	5.4M	35.2± 1.1
	Large Transformer	109M	30.5± 0.6
Personalized	TDS	5.3M	11.39
	Tiny Transformer	2.2M	9.7± 0.13
	Small Transformer	5.4M	7.9± 0.06
	Large Transformer	109M	6.8± 0.07

Table 2: Cross-user performance of transformer models trained on the *emg2qwerty* dataset, showing that [a] even the Tiny transformer models substantially outperform the TDS-ConvNet baseline in spite of having fewer parameters, and [b] the performance of the transformer model keeps improving as we increase the number of parameters in the model. For the transformer models, we report standard deviation across 6 seeds for Generic benchmark and across 3 seeds for the Personalized benchmark. The standard deviation for the baseline models is not reported in Sivakumar et al. (2024).

	Model		CER (↓%)		Abs. Gain (↑%)
Benchmark	Architecture	Params	Standard	Distilled	
Generic	Tiny	2.2M	35.9± 0.9	31.9± 0.4	4.0
	Small	5.4M	35.2± 1.1	32.7± 0.5	2.5
Personalization	Tiny	2.2M	9.7± 0.1	8.6± 0.04	1.1
	Small	5.4M	7.9± 0.06	7.1± 0.06	0.8

Table 3: Cross-user performance of small student models on the *emg2qwerty* dataset with and without distillation. Performance is measured by character error rate (CER). The 'Abs. Gain' column reflects the absolute improvement in performance from using distillation as opposed to standard supervised training for a given architecture. Personalized models are personalized from the distilled student. All models see a substantial benefit (7-11% relative improvement) from the use of the distillation loss. We report standard deviation across 3 seeds for the distillation results.

character substitutions, D is the number of deletions, and I is the number of insertions between them and N is the total number of characters in the ground-truth sequence.

4 Results

4.1 Transformer models can effectively learn from relatively small sEMG datasets

In Table 2, we compare the performance of our transformer models with the baseline TDS-ConvNet model. On the generic (zero-shot, cross-user) benchmark, even the Tiny model outperforms the TDS-ConvNet model baseline by a margin of about 20% absolute CER, in spite of having fewer than half the number of parameters as the baseline. While the performance of the Small (which is about the same size of the baseline) is not very different from that of the Tiny model, scaling the model more aggressively to the Large size does yield a further 5% improvement, reducing baseline's CER by nearly a factor of 2 (from about 55% to about 30%).

On the personalized benchmark, where the trained model is fine-tuned on a single heldout user's data, CERs are much lower across the board and therefore the absolute gains of the transformer are more modest (1.7%,

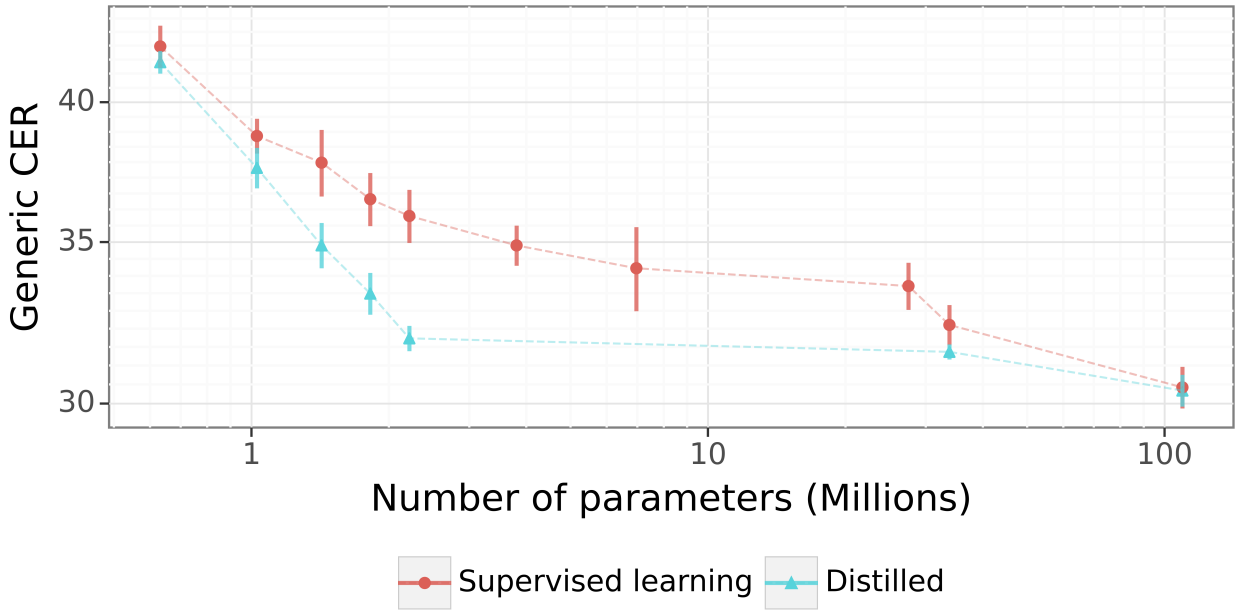

Figure 3: Scaling curve of transformers on the *emg2qwerty* dataset, showing the benefit of model size across 3 orders of magnitude from <1M to over 100M parameters, and the benefit of distillation. A few things are of note: [a] even the smallest transformer we consider here (about 600K parameters) outperforms the 5.3M parameter TDS-ConvNet baseline (55.57 CER), in spite of having almost an order of magnitude fewer parameters; and [b] the majority of distillation benefit is seen for small-but-not-too-small models, with a 2.2M parameter distilled model getting within 1.5% CER (absolute) of the top-performing model in spite of having 50x fewer parameters. Figure includes only models along the pareto front, i.e. ones which outperform others at the same or smaller parameter count. The vertical bars denote standard deviation across 6 seeds.

1.8% and 4.5% CER for Tiny, Small and Large model respectively). However, the relative magnitude of improvement is similar to that seen on the generic benchmark, especially for the largest model.

These performance gains over the baseline across all model sizes and benchmark support the usage of transformer architecture for complex sEMG tasks.

4.2 The performance of transformer models improves with scale

In Table 2, we observe that as we scale the size of the transformer model, the performance of the model continues to improve even with the same amount of data. An alternate view of this is shown in Figure 3 (red line) where we report on the 10 architectures that are on the Pareto front w.r.t. scale and performance, i.e. they perform at least as well as any model of the same or smaller size. These models show a nearly log-linear scaling curve, validating that there are performance benefits to be realized by using large transformer models for sEMG data.

One obvious challenge with the use of large transformer models is that this increases the computational overhead of the models during inference and any potential real-time usage with a HCI (e.g. to control a prosthetic, for computer text entry, or to control a cursor). Distillation techniques mitigate this limitation.

4.3 Model distillation can be applied effectively to models for sEMG

Table 3 shows the results of distilling small-capacity student models on the *emg2qwerty* dataset, using the best performing Large model as a teacher. An alternate view is in Figure 3 (turquoise line), where we see that the benefit of distillation is largest for small-but-not-too-small models. That is, for the very tiniest

models, they seem unable to fully benefit from distillation (perhaps too few layers, or too few parameters to model the teacher's distribution), while for bigger models they have enough capacity to learn the task on their own. Notably, the 2.2M parameter TINY achieves performance within 1.5% of the LARGE teacher in spite of having about 50x fewer parameters. We also report that while the LARGE teacher model takes 26.966 ms for inference over a single sample, the SMALL model takes 5.7002 ms only, thus providing a 4.7× speedup during inference. These numbers are obtained by running inference over a single sample a 1000 times to get an average runtime and then further repeating this protocol 3 times and reporting the median of the three numbers. Additional details around benchmarking are provided in the Appendix. While the specific size cutoff for a real-time model may vary, distillation provided a benefit across many small model sizes.

5 Conclusion

Our work provides a new state-of-the-art in complex sEMG decoding, specifically on the *emg2qwerty* task, which is unique in the sEMG literature for having both larger data size and higher task complexity. We demonstrated that models based on a transformer architecture are highly performant on this task, exceeding the convolutional baseline at a smaller parameter count, and continuing to improve as model size is increased an order of magnitude larger. Next, we showed that distillation of these large models can yield lightweight variants that retain strong task performance. We see this work as an early stage in a new wave of sEMG and HCI research wherein larger datasets and expressive modern architectures such as transformers will provide substantial improvements in both HCI and neuro-prosthetics domains.

Broader Impact Statement

Beyond this paper, the broader usage of sEMG, and the specific development sEMG-based textual input models, pose novel ethical and societal considerations. There are numerous societal benefits for the development of sEMG models for textual input. sEMG allows one to directly interface a person's neuromotor intent with a computing device, which can be used to, for example, develop adaptive controllers for those who struggle to use existing computer interfaces.

References

Ahmet Alkan and Mücahid Günay. Identification of emg signals using discriminant analysis and svm classifier. *Expert systems with Applications*, 39(1):44–47, 2012.

Christoph Amma, Thomas Krings, Jonas Böer, and Tanja Schultz. Advancing muscle-computer interfaces with high-density electromyography. In *Proceedings of the 33rd Annual ACM Conference on Human Factors in Computing Systems*, CHI '15, pp. 929–938, New York, NY, USA, 2015. Association for Computing Machinery. ISBN 9781450331456. doi: 10.1145/2702123.2702501. URL `https://doi.org/10.1145/2702123.2702501`.

M Atzori, A Gijsberts, C Castellini, B Caputo, AG Hager, S Elsig, G Giatsidis, F Bassetto, and H Müller. Electromyography data for non-invasive naturally-controlled robotic hand prostheses. sci data. 2014; 1: 140053, 2014.

Manfredo Atzori, Matteo Cognolato, and Henning Müller. Deep learning with convolutional neural networks applied to electromyography data: A resource for the classification of movements for prosthetic hands. *Frontiers in Neurorobotics*, 10, 2016. ISSN 1662-5218. doi: 10.3389/fnbot.2016.00009. URL `https://www.frontiersin.org/journals/neurorobotics/articles/10.3389/fnbot.2016.00009`.

Marco E. Benalcazar, Lorena Barona, Leonardo Valdivieso, Xavier Aguas, and Jonathan Zea. Emg-epn-612 dataset, November 2020. URL `https://doi.org/10.5281/zenodo.4421500`.

Cristina Brambilla, Ileana Pirovano, Robert Mihai Mira, Giovanna Rizzo, Alessandro Scano, and Alfonso Mastropietro. Combined use of emg and eeg techniques for neuromotor assessment in rehabilitative applications: A systematic review. *Sensors*, 21(21):7014, 2021.

Domenico Buongiorno, Giacomo Donato Cascarano, Irio De Feudis, Antonio Brunetti, Leonarda Carnimeo, Giovanni Dimauro, and Vitoantonio Bevilacqua. Deep learning for processing electromyographic signals: A taxonomy-based survey. *Neurocomputing*, 452:549–565, 2021. ISSN 0925-2312. doi: https://doi.org/10.1016/j.neucom.2020.06.139. URL https://www.sciencedirect.com/science/article/pii/S0925231220319020.

Yi Cai, Yifan Guo, Haotian Jiang, and Ming-Chun Huang. Machine-learning approaches for recognizing muscle activities involved in facial expressions captured by multi-channels surface electromyogram. *Smart Health*, 5:15–25, 2018.

Defang Chen, Jian-Ping Mei, Yuan Zhang, Can Wang, Zhe Wang, Yan Feng, and Chun Chen. Cross-layer distillation with semantic calibration. In *Proceedings of the AAAI conference on artificial intelligence*, volume 35, pp. 7028–7036, 2021.

Zhouping Chen, Hong Wang, Haonan Chen, and Tao Wei. Continuous motion finger joint angle estimation utilizing hybrid semg-fmg modality driven transformer-based deep learning model. *Biomedical Signal Processing and Control*, 85:105030, 2023. ISSN 1746-8094. doi: https://doi.org/10.1016/j.bspc.2023.105030. URL https://www.sciencedirect.com/science/article/pii/S1746809423004639.

Reaz H. Chowdhury, Mamun Bin Ibne Reaz, Md. Alauddin Ali, Ahmad Abu Bakar, Kasturi Chellappan, and Teck Guan Chang. Surface electromyography signal processing and classification techniques. *Sensors (Basel)*, 13(9):12431–12466, Sep 17 2013. doi: 10.3390/s130912431.

K. C. Cochrane-Snyman, T. J. Housh, C. M. Smith, E. C. Hill, N. D. Jenkins, R. J. Schmidt, and G. O. Johnson. Inter-individual variability in the patterns of responses for electromyography and mechanomyography during cycle ergometry using an rpe-clamp model. *Eur J Appl Physiol*, 116(9):1639–1649, Sep 2016. doi: 10.1007/s00421-016-3394-y. Epub 2016 Jun 20.

CTRL-labs at Reality Labs. A generic noninvasive neuromotor interface for human-computer interaction. *bioRxiv*, 2024. doi: 10.1101/2024.02.23.581779. URL https://www.biorxiv.org/content/early/2024/07/23/2024.02.23.581779.

Francesco Di Nardo, Alessandro Nocera, Alessandro Cucchiarelli, Sandro Fioretti, and Chiara Morbidoni. Machine learning for detection of muscular activity from surface emg signals. *Sensors (Basel)*, 22(9):3393, Apr 2022. doi: 10.3390/s22093393.

Ethan Eddy, Evan Campbell, Scott Bateman, and Erik Scheme. Big data in myoelectric control: large multi-user models enable robust zero-shot emg-based discrete gesture recognition. *Frontiers in Bioengineering and Biotechnology*, 12, 2024. ISSN 2296-4185. doi: 10.3389/fbioe.2024.1463377. URL https://www.frontiersin.org/journals/bioengineering-and-biotechnology/articles/10.3389/fbioe.2024.1463377.

Mekia Shigute Gaso, Selcuk Cankurt, and Abdulhamit Subasi. Electromyography signal classification using deep learning. In *2021 16th International Conference on Electronics Computer and Computation (ICECCO)*, pp. 1–6, 2021. doi: 10.1109/ICECCO53203.2021.9663803.

Ricardo V. Godoy, Gustavo J. G. Lahr, Anany Dwivedi, Tharik J. S. Reis, Paulo H. Polegato, Marcelo Becker, Glauco A. P. Caurin, and Minas Liarokapis. Electromyography-based, robust hand motion classification employing temporal multi-channel vision transformers. *IEEE Robotics and Automation Letters*, 7(4):10200–10207, 2022. doi: 10.1109/LRA.2022.3192623.

Alex Graves, Santiago Fernández, Faustino Gomez, and Jürgen Schmidhuber. Connectionist temporal classification: labelling unsegmented sequence data with recurrent neural networks. In *Proceedings of the 23rd International Conference on Machine Learning*, ICML '06, pp. 369–376, New York, NY, USA, 2006. Association for Computing Machinery. ISBN 1595933832. doi: 10.1145/1143844.1143891. URL https://doi.org/10.1145/1143844.1143891.

Awni Hannun, Ann Lee, Qiantong Xu, and Ronan Collobert. Sequence-to-sequence speech recognition with time-depth separable convolutions. *arXiv preprint arXiv:1904.02619*, 2019.

Yunan He, Osamu Fukuda, Nan Bu, Hiroshi Okumura, and Nobuhiko Yamaguchi. Surface emg pattern recognition using long short-term memory combined with multilayer perceptron. In *2018 40th Annual International Conference of the IEEE Engineering in Medicine and Biology Society (EMBC)*, pp. 5636–5639, 2018. doi: 10.1109/EMBC.2018.8513595.

Geoffrey E. Hinton, Oriol Vinyals, and Jeffrey Dean. Distilling the knowledge in a neural network. *ArXiv*, abs/1503.02531, 2015. URL https://api.semanticscholar.org/CorpusID:7200347.

Nikos Komodakis and Sergey Zagoruyko. Paying more attention to attention: improving the performance of convolutional neural networks via attention transfer. In *ICLR*, Paris, France, June 2017. URL https://enpc.hal.science/hal-01832769.

Yeonghyeon Lee, Kangwook Jang, Jahyun Goo, Youngmoon Jung, and Hoirin Kim. Fithubert: Going thinner and deeper for knowledge distillation of speech self-supervised learning, 2022. URL https://arxiv.org/abs/2207.00555.

Haoyang Li, Hongfei Ji, Jian Yu, Jie Li, Lingjing Jin, Lingyu Liu, Zhongfei Bai, and Chen Ye. A sequential learning model with gnn for eeg-emg-based stroke rehabilitation bci. *Frontiers in Neuroscience*, 17:1125230, 2023.

Wei Li, Ping Shi, and Hongliu Yu. Gesture recognition using surface electromyography and deep learning for prostheses hand: state-of-the-art, challenges, and future. *Frontiers in neuroscience*, 15:621885, 2021.

Xiaoguang Liu, Lijian Hu, Liang Tie, Li Jun, Xiaodong Wang, and Xiuling Liu. Integration of convolutional neural network and vision transformer for gesture recognition using semg. *Biomedical Signal Processing and Control*, 98:106686, 2024. ISSN 1746-8094. doi: https://doi.org/10.1016/j.bspc.2024.106686. URL https://www.sciencedirect.com/science/article/pii/S1746809424007444.

I Loshchilov. Decoupled weight decay regularization. *arXiv preprint arXiv:1711.05101*, 2017.

Ilya Loshchilov and Frank Hutter. SGDR: Stochastic gradient descent with warm restarts. In *International Conference on Learning Representations*, 2017. URL https://openreview.net/forum?id=Skq89Scxx.

Changjia Lu, Xin Xu, Yingjie Liu, Dan Li, Yue Wang, Wenhao Xian, Changbing Chen, Baichun Wei, and Jin Tian. An embedded electromyogram signal acquisition device. *Sensors*, 24(13), 2024. ISSN 1424-8220. doi: 10.3390/s24134106. URL https://www.mdpi.com/1424-8220/24/13/4106.

Behnam Mokhlesabadifarahani and V. K. Gunjan. *EMG Signals Characterization in Three States of Contraction by Fuzzy Network and Feature Extraction*. Springer Singapore Pte. Limited, 2015th edition, 2015. doi: 10.1007/978-981-287-320-0.

Shion Morikawa, Shin-ichi Ito, Momoyo Ito, and Minoru Fukumi. Personal authentication by lips emg using dry electrode and cnn. In *2018 IEEE International Conference on Internet of Things and Intelligence System (IOTAIS)*, pp. 180–183, 2018. doi: 10.1109/IOTAIS.2018.8600859.

Max Ortiz-Catalan, Rickard Brånemark, and Bo Håkansson. BioPatRec: A modular research platform for the control of artificial limbs based on pattern recognition algorithms. *Source Code for Biology and Medicine*, 8:11, 2013. doi: 10.1186/1751-0473-8-11.

Mehmet Akif Ozdemir, Deniz Hande Kisa, Onan Guren, Aytug Onan, and Aydin Akan. Emg based hand gesture recognition using deep learning. In *2020 Medical Technologies Congress (TIPTEKNO)*, pp. 1–4, 2020. doi: 10.1109/TIPTEKNO50054.2020.9299264.

Wonpyo Park, Dongju Kim, Yan Lu, and Minsu Cho. Relational knowledge distillation. In *Proceedings of the IEEE/CVF conference on computer vision and pattern recognition*, pp. 3967–3976, 2019.

Yifan Peng, Yui Sudo, Shakeel Muhammad, and Shinji Watanabe. Dphubert: Joint distillation and pruning of self-supervised speech models, 2023. URL https://arxiv.org/abs/2305.17651.

Robert Plonsey and Robert C. Barr. *Bioelectricity: A quantitative approach*. Springer, 2007.

Reiner Pope, Sholto Douglas, Aakanksha Chowdhery, Jacob Devlin, James Bradbury, Jonathan Heek, Kefan Xiao, Shivani Agrawal, and Jeff Dean. Efficiently scaling transformer inference. *Proceedings of Machine Learning and Systems*, 5:606–624, 2023.

Nur Achmad Sulistyo Putro, Cries Avian, Setya Widyawan Prakosa, Muhammad Izzuddin Mahali, and Jenq-Shiou Leu. Estimating finger joint angles by surface emg signal using feature extraction and transformer-based deep learning model. *Biomedical Signal Processing and Control*, 87:105447, 2024. ISSN 1746-8094. doi: https://doi.org/10.1016/j.bspc.2023.105447. URL https://www.sciencedirect.com/science/article/pii/S1746809423008807.

Elahe Rahimian, Soheil Zabihi, Amir Asif, Dario Farina, S. Farokh Atashzar, and Arash Mohammadi. Temgnet: Deep transformer-based decoding of upperlimb semg for hand gestures recognition, 2021. URL https://arxiv.org/abs/2109.12379.

Parul Rani, Sidharth Pancholi, Vikash Shaw, Manfredo Atzori, and Sanjeev Kumar. Enhancing gesture classification using active emg band and advanced feature extraction technique. *IEEE Sensors Journal*, 24(4):5246–5255, 2024. doi: 10.1109/JSEN.2023.3344700.

Adriana Romero, Nicolas Ballas, Samira Ebrahimi Kahou, Antoine Chassang, Carlo Gatta, and Yoshua Bengio. Fitnets: Hints for thin deep nets. *ICLR*, abs/1412.6550, 2015. URL https://api.semanticscholar.org/CorpusID:2723173.

Qingshan She, Zhizeng Luo, Ming Meng, and Ping Xu. Multiple kernel learning svm-based emg pattern classification for lower limb control. In *2010 11th International Conference on Control Automation Robotics & Vision*, pp. 2109–2113. IEEE, 2010.

Ryohei Shioji, Shin ichi Ito, Momoyo Ito, and Minoru Fukumi. Personal authentication and hand motion recognition based on wrist emg analysis by a convolutional neural network. *2018 IEEE International Conference on Internet of Things and Intelligence System (IOTAIS)*, pp. 184–188, 2018. URL https://api.semanticscholar.org/CorpusID:57753769.

Viswanath Sivakumar, Jeffrey Seely, Alan Du, Sean Bittner, Adam Berenzweig, Anuoluwapo Bolarinwa, Alex Gramfort, and Michael Mandel. EMG2QWERTY: A Large Dataset with Baselines for Touch Typing using Surface Electromyography. In *Proceedings of the Neural Information Processing Systems (NeurIPS)*, 2024.

Jiaxi Tang, Rakesh Shivanna, Zhe Zhao, Dong Lin, Anima Singh, Ed H Chi, and Sagar Jain. Understanding and improving knowledge distillation. *arXiv preprint arXiv:2002.03532*, 2020.

Frederick Tung and Greg Mori. Similarity-preserving knowledge distillation. In *Proceedings of the IEEE/CVF international conference on computer vision*, pp. 1365–1374, 2019.

A Vaswani, N Shazeer, N Parmar, J Uszkoreit, L Jones, A Gomez, L Kaiser, and I Polosukhin. Attention is all you need. In *NIPS*, 2017.

Michael Wand and Jürgen Schmidhuber. Deep neural network frontend for continuous emg-based speech recognition. In *Interspeech*, pp. 3032–3036, 2016.

Yujin Wang, Changli Tang, Ziyang Ma, Zhisheng Zheng, Xie Chen, and Wei-Qiang Zhang. Exploring effective distillation of self-supervised speech models for automatic speech recognition, 2023. URL https://arxiv.org/abs/2210.15631.

L. N. Wimalasena, J. F. Braun, M. R. Keshtkaran, D. Hofmann, J. Á. Gallego, C. Alessandro, M. C. Tresch, L. E. Miller, and C. Pandarinath. Estimating muscle activation from emg using deep learning-based dynamical systems models. *J Neural Eng*, 19(3), May 2022. doi: 10.1088/1741-2552/ac6369.

Peng Xia, Jie Hu, and Yinghong Peng. Emg-based estimation of limb movement using deep learning with recurrent convolutional neural networks. *Artificial Organs*, 42(5):E67–E77, 2018. doi: https://doi.org/10.1111/aor.13004. URL https://onlinelibrary.wiley.com/doi/abs/10.1111/aor.13004.

Zheng Xu, Yen-Chang Hsu, and Jiawei Huang. Training shallow and thin networks for acceleration via knowledge distillation with conditional adversarial networks, 2018. URL https://arxiv.org/abs/1709.00513.

Chia-Yen Yang, Pin-Chen Chen, and Wen-Chen Huang. Cross-domain transfer of eeg to eeg or ecg learning for cnn classification models. *Sensors*, 23(5):2458, 2023.

Soheil Zabihi, Elahe Rahimian, Amir Asif, and Arash Mohammadi. Trahgr: Transformer for hand gesture recognition via electromyography. *IEEE Transactions on Neural Systems and Rehabilitation Engineering*, 31:4211–4224, 2023. doi: 10.1109/TNSRE.2023.3324252.

Wenli Zhang, Tingsong Zhao, Jianyi Zhang, and Yufei Wang. Lst-emg-net: Long short-term transformer feature fusion network for semg gesture recognition. *Frontiers in Neurorobotics*, 17, 2023. ISSN 1662-5218. doi: 10.3389/fnbot.2023.1127338. URL https://www.frontiersin.org/journals/neurorobotics/articles/10.3389/fnbot.2023.1127338.

Borui Zhao, Quan Cui, Renjie Song, Yiyu Qiu, and Jiajun Liang. Decoupled knowledge distillation. In *Proceedings of the IEEE/CVF Conference on computer vision and pattern recognition*, pp. 11953–11962, 2022.

Appendix

The appendix is organized as follows: In Section A we lay out all of the experimental details of the results presented in this work and in Section B we show additional results which were not presented in the main text.

A Experimental details

We describe the hyperparameters and model details in the following subsections. We provide constant hyperparameters in one table and hyperparameters that are subject to vary in a separate table. In Section A.2, we list the hyperparameters of the supervised learning models presented in this paper, i.e., without distillation signal; in Section A.3, we list the hyperparameters of the distilled models; and in Section A.4 we describe the hyperparameters of the personalization experiment.

A.1 Dataset details

In Table 4, we detail the aggregated statistics of the *emg2qwerty* dataset.

Table 4: *emg2qwerty* dataset statistics

Total subjects	108
Total sessions	1,135
Avg sessions per subject	10
Max sessions per subject	18
Min sessions per subject	1
Total duration	346.4 hours
Avg duration per subject	3.2 hours
Max duration per subject	6.5 hours
Min duration per subject	15.3 minutes
Avg duration per session	18.0 minutes
Max duration per session	47.5 minutes
Min duration per session	9.5 minutes
Avg typing rate per subject	265 keys/min
Max typing rate per subject	439 keys/min
Min typing rate per subject	130 keys/min
Total keystrokes	5,262,671

A.2 Supervised learning details

In the supervised learning experiments, we train a grid of model with sizes $[128, 256, 512, 1024]$ transformer hidden representation size and $[2, 4, 6, 8, 10]$ layers. For each of the hidden representation sizes, we set the transformer feed-forward dimension such that the feed-forward ratio ($d_{\text{ff}}/d_{\text{hidden}}$) is maintained at 4. For each of these configuration, we launch multiple learning rates ($[3e-3, 1e-3, 3e-4, 1e-4]$) across 6 different seeds. Seeding is used to determine dataloading order and model initialization. We train all models to completion (200 epochs) and evaluate the model on the training and validation at the end of every epoch. For each model, we artificially early-stop the model post-hoc by choosing the epoch with the lowest validation CER and record the test set CER of the model for this epoch. The rest of the training-related hyperparameters (specifically dropout probabilities, weight decay and learning rate schedule) were chosen according to best values in prior experimentation with a fixed model size.

We aggregate the results by first taking the validation and test CER averages across seeds, then pick the best aggregated validation learning rate value and report the average and standard deviation of the test results. The chosen hyperparameters are reported in Table 6 and the test CER reported in Table 11.

Table 5: Supervised learning task details and hyperparameters held constant for models from Table 11.

Data	Input sEMG channels	32
	Window length	8000
	Padding	$[1800, 200]$
Architecture	Featurizer channels	$[128, 64, 64]$
	Featurizer kernels	$[11, 3, 3]$
	Featurizer strides	$[5, 2, 2]$
	Encoder feed-forward ratio	4
	Encoder convolutional dim	64
	Encoder attentions heads	16
	Tokenizer	Character-level
	Vocab size	99
	Encoder hidden, attention and activation dropout	0.2
	Encoder feature projection dropout	0.2
	Encoder final layer dropout	0.2
Training	Epochs	200.0
	Effective batch size	640
	Encoder causal attention	True
Optimizer	Learning rate schedule	linear warmup + cosine decay
	Learning rate warmup ratio	0.05
	Weight decay	0.2
	CTC zero infinity	True
	Gradient clipping	0.1
Software	Torch version	2.3.1+cu121
	Transformers version	4.36.2

Table 6: Supervised learning task hyperparameters that vary for models from Table 11.

Architecture	Encoder hidden size	Encoder layers	Optimizer learning rate
	128	2	1e-03
	128	4	1e-03
	128	6	1e-03
	128	8	1e-03
Tiny	**128**	**10**	**1e-03**
	256	2	1e-03
	256	4	1e-03
Small	**256**	**6**	**1e-03**
	256	8	1e-03
	256	10	3e-04
	512	2	1e-03
	512	4	3e-04
	512	6	3e-04
	512	8	3e-04
	512	10	3e-04
	1024	2	1e-03
	1024	4	3e-04
	1024	6	3e-04
Large	**1024**	**8**	**3e-04**
	1024	10	3e-04

A.3 Distillation details

In the distillation experiments, we train the same grid of model width and depth as in the supervised learning experiments (Section A.2) to use as the student model. The teacher model is chosen by picking the best performing model from the best model configuration from the supervised learning experiments in Table 11. For each of the hidden representation sizes of the student model, we set the transformer feed-forward dimension such that the feed-forward ratio ($d_{\text{ff}}/d_{\text{hidden}}$) is maintained at 4. For each of these configurations, we launch multiple learning rates ($[3e-3, 1e-3, 3e-4]$) across 3 different seeds. Seeding is used to determine dataloading order and model weight initialization. We train all models to completion (200 epochs) and evaluate the model on the training and validation at the end of every epoch. For each model, we select the checkpoint with the lowest validation CER and record the test set CER of this checkpoint. The rest of the training-related hyperparameters (specifically distillation penalty weight, student dropout probabilities, weight decay and learning rate schedule) were chosen according to best validation metrics in prior experimentation with a fixed model size.

We aggregate the results by first taking the validation and test CER averages across seeds, then pick the best aggregated validation learning rate value and report the average and standard deviation on the test results. The chosen hyperparameters are reported in Table 8 and the test CER reported in Table 12.

Table 7: Distillation task details and hyperparameters held constant for models from Table 12.

Data	Input sEMG channels	32
	Window length	8000
	Padding	[1800, 200]
Student arch.	Featurizer channels	[128, 64, 64]
	Featurizer kernels	[11, 3, 3]
	Featurizer strides	[5, 2, 2]
	Encoder convolutional dim	[64]
	Encoder attentions heads	16
	Text Tokenizer	Character-level
	Vocab size	99
	Encoder hidden, attention and activation dropout	0.2
	Encoder feature projection dropout	0.2
	Encoder final layer dropout	0.2
Teacher arch.	Featurizer channels	[128, 64, 64]
	Featurizer kernels	[11, 3, 3]
	Featurizer strides	[5, 2, 2]
	Encoder hidden size	1024
	Encoder feed-forward ratio	4
	Encoder layers	8
	Encoder convolutional dim	[64]
	Encoder attentions heads	16
	Text Tokenizer	Character-level
	Vocab size	99
	Encoder hidden, attention and activation dropout	0.0
	Encoder feature projection dropout	0.0
	Encoder final layer dropout	0.0
Training	Epochs	200
	Effective batch size	640
	Encoder causal attention	True
Optimizer	Learning rate schedule	linear warmup + cosine decay
	Learning rate warmup ratio	0.05
	Weight decay	0.1
	CTC zero infinity	True
	Gradient clipping	0.1
	Distillation loss weight	0.5
	Distillation loss (logits)	Cross Entropy
Software	Torch version	2.3.1+cu121
	Transformers version	4.36.2

Table 8: Distillation hyperparameters that vary for models from Table 12.

Student arch.	Student encoder hidden size	Student encoder layers	Optimizer learning rate
	128	2	1e-03
	128	4	1e-03
	128	6	1e-03
	128	8	1e-03
Tiny	128	10	1e-03
	256	2	1e-03
	256	4	1e-03
Small	256	6	1e-03
	256	8	1e-03
	256	10	1e-03
	512	2	3e-03
	512	4	1e-03
	512	6	1e-03
	512	8	1e-03
	512	10	3e-04
	1024	2	1e-03
	1024	4	1e-03
	1024	6	3e-04
Large	1024	8	3e-04
	1024	10	3e-04

A.4 Personalization details

In the personalization experiments, we focus on our three highlighted architecture configurations, i.e., Tiny, Small and Large. For each architecture, we pick three models from the supervised learning experiments, irrespective of hyperparameters and seeds, according to the best validation performance. We refer to these three models as seed A, B and C. For the Tiny and Small architecture, we repeat this procedure with the distillation set of experiments. We refer to these models as being from the "Distillation" origin, as opposed to the "Supervised" origin for the models taken from the supervised learning experiments. For each of those models, we initialize the personalization models from the chosen checkpoint and we launch multiple learning rates ($[3e-3, 1e-3, 3e-4]$) across 3 different seeds for each of the 8 personalization users. Seeding is used to determine dataloading order and model weight initialization. We train all models to completion (100 epochs) and evaluate the model on the training and validation sets at the end of every epoch. For each model, we select the checkpoint with the lowest validation CER and record the test set CER of this checkpoint. The rest of the training-related hyperparameters (specifically student dropout probabilities, weight decay and learning rate schedule) were chosen according to best validation metrics in prior experimentation with a fixed model size.

We aggregate the results by first taking the validation and test CER averages across the personalized users and seeds. We then pick the best aggregated validation learning rate value and report the average and standard deviation on the test results. The chosen hyperparameters are reported in Table 10 and the test CER reported in Table 13. Table 10 also reports the supervised or distillation learning rate used by the seed generic model the personalized was initialized from.

Table 9: Personalization task details and hyperparameters held constant for models from Table 13.

Data	Input sEMG channels	32
	Window length	8000
	Padding	[1800, 200]
Architecture	Featurizer channels	[128, 64, 64]
	Featurizer kernels	[11, 3, 3]
	Featurizer strides	[5, 2, 2]
	Encoder feed-forward ratio	4
	Encoder convolutional dim	[64]
	Encoder attentions heads	16
	Tokenizer	Character-level
	Vocab size	99
	Encoder hidden, attention and activation dropout	0.2
	Encoder feature projection dropout	0.2
	Encoder final layer dropout	0.2
Training	Epochs	100.0
	Effective batch size	640
	Encoder causal attention	True
Optimizer	Learning rate schedule	linear warmup + cosine decay
	Learning rate warmup ratio	0.05
	Weight decay	0.0
	Training warmup ratio	0.05
	CTC zero infinity	True
	Gradient clipping	0.1
Software	Torch version	2.3.1+cu121
	Transformers version	4.36.2

Table 10: Personalization hyperparameters that vary for models from Table 13.

Architecture	Init. origin	Init. seed	Generic training lr	Personalization training lr
Tiny	Distillation	seed A	1e-03	3e-04
Tiny	Distillation	seed B	1e-03	3e-04
Tiny	Distillation	seed C	1e-03	3e-04
Tiny	Supervised	seed A	1e-03	3e-04
Tiny	Supervised	seed B	1e-03	3e-04
Tiny	Supervised	seed C	1e-03	3e-04
Small	Distillation	seed A	1e-03	3e-04
Small	Distillation	seed B	1e-03	3e-04
Small	Distillation	seed C	1e-03	3e-04
Small	Supervised	seed A	1e-03	3e-04
Small	Supervised	seed B	3e-04	3e-04
Small	Supervised	seed C	3e-04	3e-04
Large	Supervised	seed A	3e-04	3e-05
Large	Supervised	seed B	3e-04	1e-04
Large	Supervised	seed C	3e-04	1e-04

B Additional results

In Section B.1, we show training curve samples from our experiments. In Section B.2, we show the results for the full model scaling grid we explored. In Section B.3, we present measures of the inference speed of our models.

B.1 Sample training metrics

We show training curves from some of our experiments assist others to more easily reproduce our results. In Figure 4 and 5, we show training loss along with validation (cross-session) and test (cross-user) generic CER for the supervised and distillation tasks respectively. In Figure 6, we show personalization training loss and personalized CER for three of the eight personalization users.

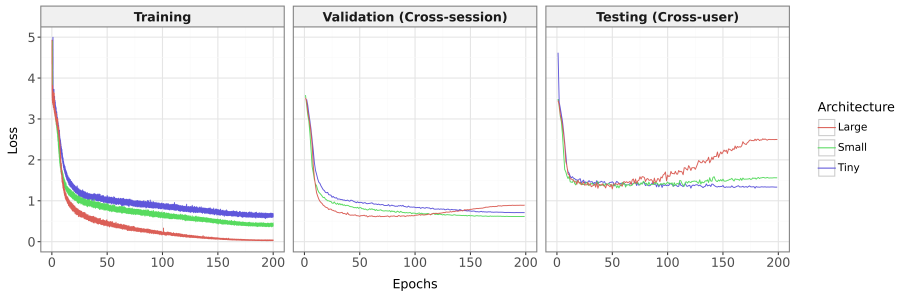

(a) Loss

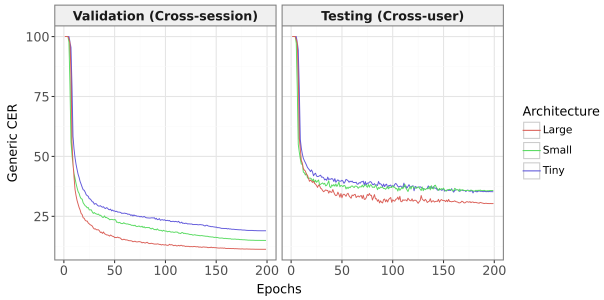

(b) Generic CER

Figure 4: Supervised training sample training curves for the Tiny, Small, Large architecture. Validation is done with unseen sessions from the training users while testing is done across unseen sessions from the unseen users.

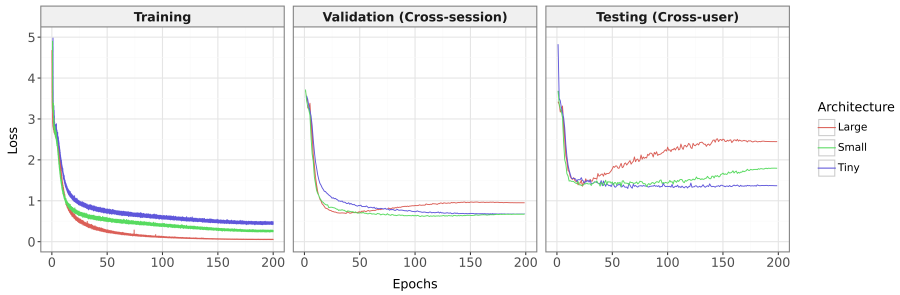

(a) Loss

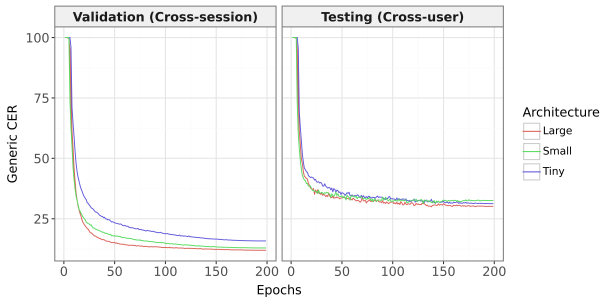

(b) Generic CER

Figure 5: Distillation training sample training curves for the Tiny, Small, Large architecture. Validation is done with unseen sessions from the training users while testing is done across unseen sessions from the unseen users.

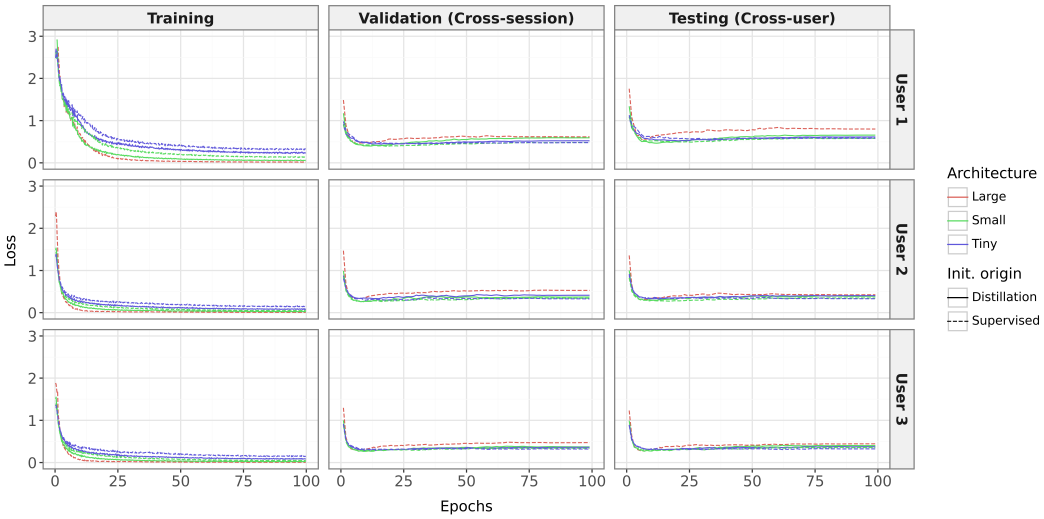

(a) Loss

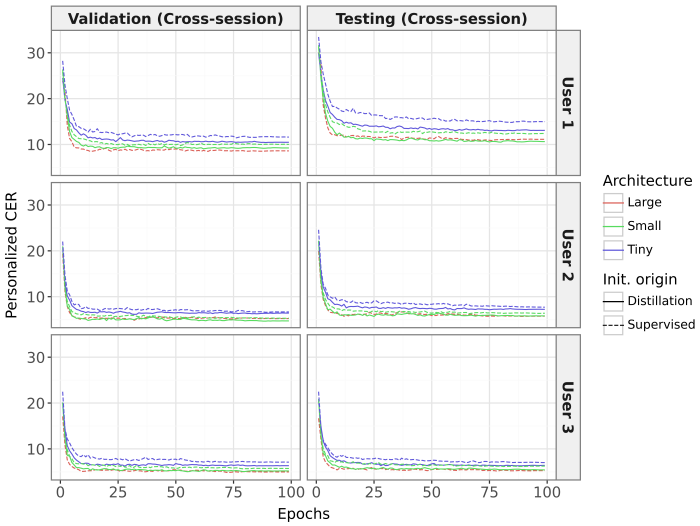

(b) Generic CER

Figure 6: Personalization training sample training curves for the Tiny, Small, Large architecture. For the Tiny and Small architectures we show the separate curves for initializing the model coming from supervised training and distillation training. We show the training curves for three of the eight personalization users. Both validation and testing is done with unseen sessions from the (single) training user.

B.2 Full model grid scaling results

Model architecture exploration In Figure 7, we show the results for all model shapes investigated in this work. We use this grid of shapes to compute the pareto front, i.e. ones which outperform others at the same or smaller parameter count, presented in Figure 3. Our grid extends from an transformer hidden representation size of 128 to 1024 and a number of transformer layer from 2 to 10. The featurization module which first converts raw EMG into features to feed into the transformer is kept fixed for all models (see Table 5 and Table 7 for the exact configuration). The CER results for generic models (from Figure 7) along with their standard deviation can be found in Table 11 for supervised learning and Table 12 for distilled models.

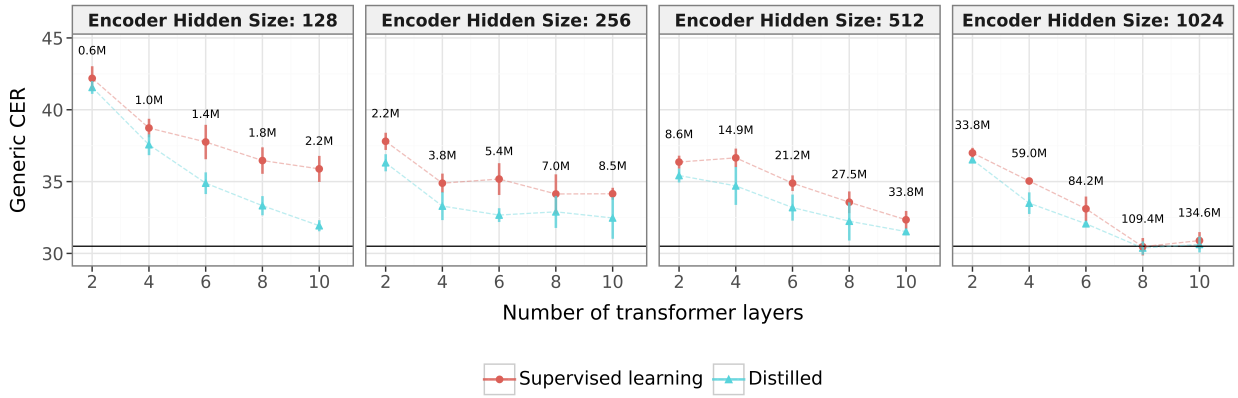

Figure 7: Supervised learning and distilled results on the *emg2qwerty* dataset across multiple model hidden representation size and number of layers. The total number of parameters of the networks are annotated for each configuration. The performance of the teacher model (LARGE architecture) for the distillation training is highlighted by the horizontal line. The vertical bars denote standard deviation across 6 seeds.

Distillation improvement In Figure 8, we show the generic CER improvement observed through distillation across transformer model width and depth.

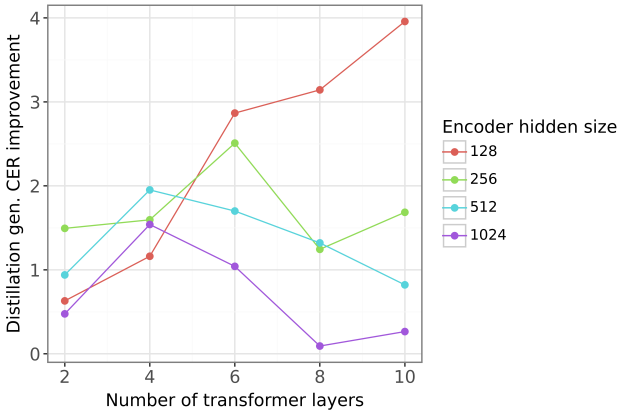

Figure 8: Performance improvement from distillation over supervised learning on the *emg2qwerty* dataset across multiple model hidden representation size and number of layers.

Numerical results Following is the full set of numerical performance reported in this paper. In Table 11 and 12 we annotate the TINY, SMALL and LARGE architecture which corresponds to the architecture highlighted in Table 3 of the main paper.

Table 11: Numerical generic CER and their standard deviation for supervised learning analysis. Hyperparameters provided in Section A.2. The specific named architectures from the main text are highlighted in bold.

Architecture	Encoder hidden size	Encoder layers	Model params	Generic CER
	128	2	631523	42.19 ±0.85
	128	4	1028067	38.73 ±0.64
	128	6	1424611	37.76 ±1.20
	128	8	1821155	36.46 ±0.92
Tiny	**128**	**10**	**2217699**	**35.88 ±0.91**
	256	2	2229091	37.81 ±0.60
	256	4	3808611	34.89 ±0.67
Small	**256**	**6**	**5388131**	**35.18 ±1.11**
	256	8	6967651	34.14 ±1.37
	256	10	8547171	34.15 ±0.42
	512	2	8569955	36.36 ±0.44
	512	4	14874723	36.65 ±0.65
	512	6	21179491	34.89 ±0.54
	512	8	27484259	33.56 ±0.75
	512	10	33789027	32.34 ±0.62
	1024	2	33834595	37.00 ±0.36
	1024	4	59027043	35.04 ±0.19
	1024	6	84219491	33.10 ±0.85
Large	**1024**	**8**	**109411939**	**30.47 ±0.61**
	1024	10	134604387	30.89 ±0.60

Table 12: Numerical generic CER and their standard deviation for distillation analysis. Encoder hidden sizes and layers represents the student encoder sizes. The teacher follows the Large architecture. Hyperparameters are provided in Section A.3

.

Student arch.	Student encoder hidden size	Student encoder layers	Model params	Generic CER
	128	2	631523	41.56 ±0.45
	128	4	1028067	37.57 ±0.72
	128	6	1424611	34.89 ±0.76
	128	8	1821155	33.32 ±0.67
Tiny	**128**	**10**	**2217699**	**31.93 ±0.39**
	256	2	2229091	36.31 ±0.60
	256	4	3808611	33.29 ±0.98
Small	**256**	**6**	**5388131**	**32.67 ±0.48**
	256	8	6967651	32.89 ±1.11
	256	10	8547171	32.47 ±1.45
	512	2	8569955	35.42 ±0.48
	512	4	14874723	34.70 ±1.32
	512	6	21179491	33.19 ±0.91
	512	8	27484259	32.24 ±1.34
	512	10	33789027	31.52 ±0.23
	1024	2	33834595	36.52 ±0.19
	1024	4	59027043	33.50 ±0.75
	1024	6	84219491	32.06 ±0.22
Large	**1024**	**8**	**109411939**	**30.38 ±0.46**
	1024	10	134604387	30.63 ±0.56

Table 14: Inference speed of highlighted model sizes (per 4 second window).

Architecture	Encoder hidden size	Encoder layers	Params	Inference speed (ms)
TINY TRANSFORMER	128	10	2.2M	6.1
SMALL TRANSFORMER	256	6	5.4M	5.7
LARGE TRANSFORMER	1024	8	109M	27.0

Table 13: Numerical generic CER and their standard deviation for the personalization results with varying model initialization. The initialization origin column represents whether the generic model used as initialization for the personalized model has been trained through *Supervised* learning (i.e., without distillation loss) or through *Distillation*. The initialization seed column represents distinction between different models with the same architecture, but trained on different seeds or different hyperparameters, selected by choosing the best validation performance among the all the models trained. Hyperparameters provided in Section A.4.

Architecture	Init. origin	Init. seed	Model params	Generic CER
Tiny	Distillation	seed A	2217699	8.64 ±0.04
Tiny	Distillation	seed B	2217699	8.65 ±0.02
Tiny	Distillation	seed C	2217699	8.91 ±0.06
Tiny	Supervised	seed A	2217699	9.72 ±0.13
Tiny	Supervised	seed B	2217699	9.91 ±0.13
Tiny	Supervised	seed C	2217699	10.36 ±0.02
Small	Distillation	seed A	5388131	7.07 ±0.06
Small	Distillation	seed B	5388131	7.02 ±0.03
Small	Distillation	seed C	5388131	7.16 ±0.01
Small	Supervised	seed A	5388131	7.94 ±0.06
Small	Supervised	seed B	5388131	9.78 ±0.07
Small	Supervised	seed C	5388131	9.20 ±0.06
Large	Supervised	seed A	109411939	6.81 ±0.07
Large	Supervised	seed B	109411939	6.48 ±0.02
Large	Supervised	seed C	109411939	6.54 ±0.08

B.3 Inference speed

We measured the inference speed of the highlighted TINY, SMALL and LARGE in Table 2 model architecture to assess their viability to be run in real time and to see how much model scale influences inference speeds. We present the inference speeds in Table 14.

Naive streaming inference In the most naive case of streaming inference, we pass a full window length of data (4 second in emg2qwerty) to the model and use exclusively the final prediction, then repeat this process for the next prediction.

Applying this naive streaming inference paradigm to single-window inference speed in Table 14 tells us that the LARGE architecture could not be inferable in real-time due to the maximum inference frequency being approximately $f = \frac{1}{27\text{ms}} = 37\text{Hz}$.

Note that under this setting one can trade off latency with inference speed, for example by using the last n predictions from a window as predictions, which alleviates the requirements on inference speed by nx at the cost of increasing latency of the output by nx.

Accelerated streaming inference In a more sophisticated implementation of streaming inference, one could further improve the performance of the models by using optimizations like KV Caching (Pope et al., 2023) or designing custom kernels. These techniques are outside the scope of our work.